Figure 2. The determination of IL-28B gene structure and UTR region. *IL-28A/B* cDNA was isolated using a complete cDNA cloning method and the entire sequences were determined using HeLa, MT-2, and Raji cell lines and PBMC from healthy volunteers. (A) 5′- and 3′-RACE analyses were used to determine the complete sequence of *IL-28A/B* mRNA after LPS stimulation (3 μg/mL) for 4 h following IFN-α treatment (100 U/mL) for 16 h. A representative example of agarose gel electrophoresis is shown for the non-stimulated control (NC). PCR products were inserted into the cloning vector and 6 clones of 5′- and 3′-RACE were analyzed by sequencing. (B) mRNA sequences of the 5′ terminal region were aligned using CCDS retrieved from NCBI and RACE data of *IL-28A/B*. The upper two sequences are reference sequences from the NCBI CCDS and the lower two are representative sequences of *IL-28A* and *28B* obtained from 5′-RACE. The underlined triplet indicates the start codon of each gene and arrow shows the splice junctions. (C) mRNA sequences of the 3′ terminal region were aligned using CCDS retrieved from NCBI and RACE data from *IL-28A/B*. The double-underlined triplet indicates the stop codon of each gene and arrows show the splice junctions. The polyA signal and representative site of polyadenylation also are shown. (D) The derived gene structure of the *IL-28B* is shown with the significant SNPs. The location of SNP No. 3 was changed from the regulatory to an intron region. The transcription start site (TSS) is found behind SNP No. 2.
doi:10.1371/journal.pone.0026620.g002

20 pmol of each primer, 5×PrimeSTAR GXL Buffer, 2.5 mM each deoxynucleotide triphosphates, and 1.25 units of PrimeStar GXL DNA polymerase (TAKARA Bio Inc, Tokyo, Japan). The primer pair, G1 and G2 (listed in Table S1), was used for the simultaneous amplification of the *IL-28A* and *28B* regulatory regions. The PCR conditions were as follows: 30 cycles of 10 s at 98°C, and 120 s at 68°C in addition of initial denaturation at 98°C for 5 min and a final extension at 68°C for 10 min. To separate the *IL-28A* amplicon from that of *IL-28B*, 10 μl of PCR products were analyzed using agarose gel electrophoresis and extracted with QIAquick Gel Extraction Kit (Qiagen). Each extracted product was analyzed by direct sequencing using Seq1 and Seq2 primers (Table S1). For further testing of the TA repeat, heterozygous samples were cloned into the pGEM-Teasy vector to count the number of TA repeats in each allele. Six clones were isolated and subjected to sequencing analysis using the primers described above.

Reporter assay

Luciferase assays of recombinant protein were performed using Dual-Glo Luciferase reporter assay system (Promega, Fitchburg, WI). In toll-like receptor (TLR)-stimulated experiments Raji cells were transfected and left for 16 h with 100 U/mL of IFN-α, then were exposed to LPS (3 μg/ml) for 4 h before harvesting. For assessments of recombinant protein, HeLa cells were transfected with pISRE-Luc and pGL4.74, and were harvested 24 h after IFN-α or λ treatment. The chemiluminescence was measured by SpectraMax L (Molecular Devices, Sunnyvale, CA). Firefly luciferase activity was normalized to Renilla activity to adjust for transfection efficiency.

Real-time PCR detection

Jurkat cells were transfected with the *IL-28B* expression vector harboring a FLAG sequence derived from the natural promoter (pdCMV/MA, mi, or AS). To induce IL-28B expression, TLR and IFN-α stimulation was given as described above. FLAG and glyceraldehyde-3-phosphate dehydrogenase (GAPDH) mRNA expression were measured using a real-time PCR performed on ABI Prism 7700 sequence detection system (Applied Biosystems) using primer sets (Table S1) after total RNA extraction and reverse transcription (RT) using an RT kit and TaqMan Universal PCR master mix (both Applied Biosystems), according to the manufacturer's manual. Relative gene expression was calculated as a fold induction compared to the control. Data were analyzed by the 2[-Delta Delta C(t)] method using Sequence Detector version 1.7 software (Applied Biosystems) [18] and were normalized using human GAPDH. A standard curve was prepared by serial 10-fold dilutions of human cDNA or FLAG plasmid. The curve was linear over 7 logs with a 0.998 correlation coefficient.

Statistical Analysis

Statistical analyses were conducted by using SPSS software package (SPSS 18J, SPSS, Chicago, IL) and Microsoft Excel 2007 (Microsoft co., Redmond, WA). Discrete variables were evaluated by Fisher's exact probability test. The P values were calculated by two-tailed student's t-tests for continuous data and chi-square test for categorical data, and those of less than 0.05 were considered as statistically significant.

Results

The identification of IL-28B gene structure

To define the human *IL-28A* or *IL-28B* gene structure, 5′-RACE and 3′-RACE were performed on total extracted RNA from HeLa, MT-2, Raji, HuH7 cells, and PBMCs from healthy volunteers (Fig. 2A). The sequences obtained matched the genomic contig of AC011445, which contains the sequence of *IL-28A* and *IL-28B* in forward and reverse orientations, respectively. All intron/exon junctions conformed to the canonical GT-AG rule. After stimulation of cells with LPS (3 μg/ml) for 4 h following IFN-α treatment (100 U/mL) for 16 h, *IL-28A/B* transcripts were detected in RACE experiments, but these were not detected in unstimulated cells. The representative TSSs are shown in Fig. 2B and showed little variation among cloned mRNA transcripts. The same 3′-UTR fragment also was detected without any intron in the 3′-RACE experiments (Fig. 2C). A polyadenylation signal (AAAUAAA), located in the 3′-UTR, was found upstream of the polyadenylation site in all samples. All sequences from the transcripts were aligned on the 5′-UTR, the six exons, and the 3′-UTR region of *IL-28A/B*. No different mRNA transcripts of *IL-28A/B* were found in our experiment. Taken together, the *IL-28B* gene structure comprised six exons (see Fig. 2D), and the location of SNP no. 3 (rs28416813) is in an intron, rather than a regulatory region (Table 1).

The effect of regulatory SNPs on promoter activity

Because the TSS was upstream of the position described in previous reports (Fig. 2), two rSNPs (rs72258881 and rs4803219) in the regulatory region were more specifically located in the TSS. A luciferase reporter approach was used to assess the effects of the two rSNPs on promoter activity. Luciferase vectors harboring the rSNPs were constructed and used for transfections (Fig. 3A). The promoter activities of the constructs were measured after stimulation with LPS (3 μg/ml) for 4 h following IFN-α treatment (100 U/mL) for 16 h. The transcriptional activity of constructions harboring the $(TA)_{11}$ mutation was reduced (Fig. 3B). Substitution in the rSNP (rs4803219) showed little effect on the transcriptional activity, whereas the number of TA repeats could be responsible for the putative region controlling basal transcription. To confirm the transcriptional activity, Jurkat cells were transfected with full length constructs expressing the FLAG sequence under the control of the natural promoter (Fig. 3C). To avoid the detection of endogenous mRNA, the mRNA with the FLAG sequence was specifically detected by real time PCR using the FLAG primer. The constructs harboring $(TA)_{11}$ yielded lower expression levels

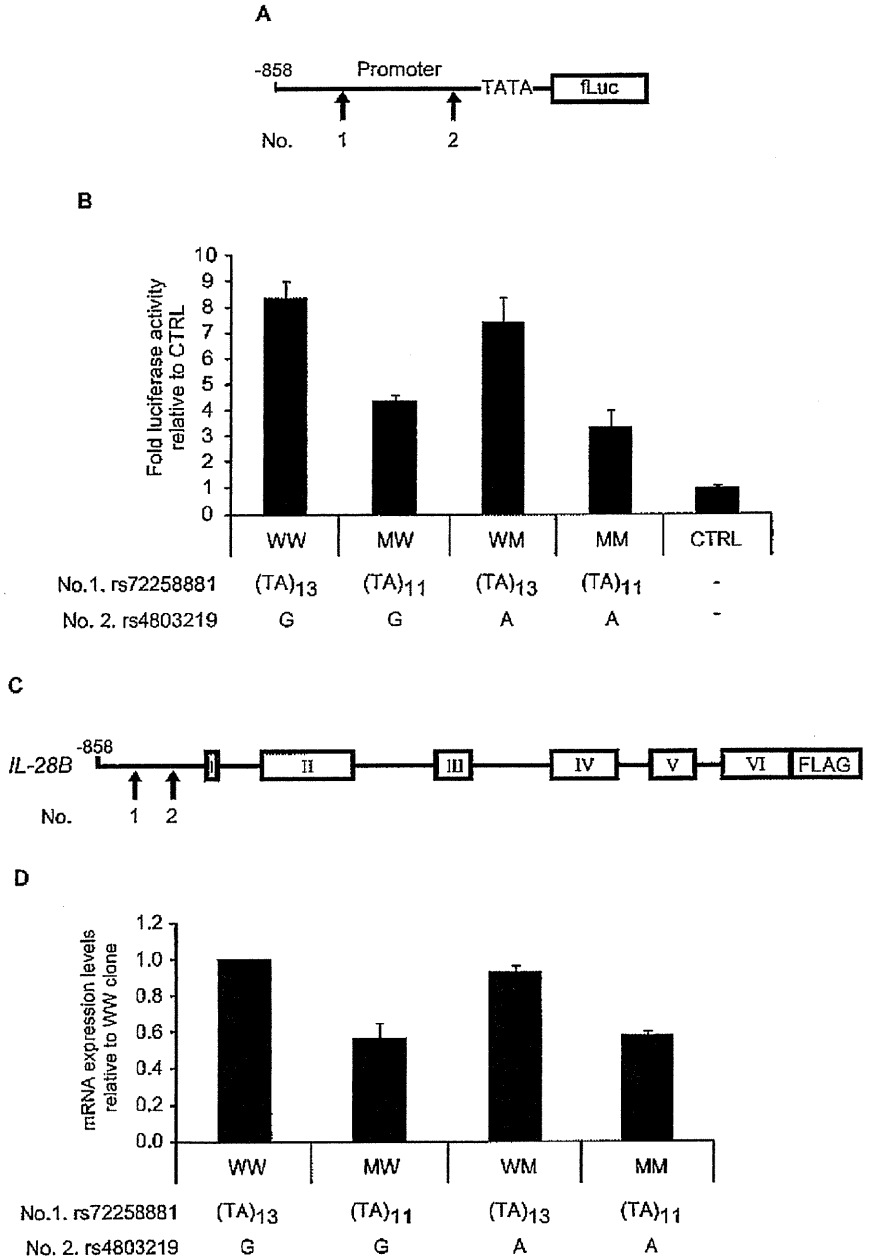

Figure 3. Transcriptional activity of the IL-28B promoter region compared between major and minor alleles. (A) The pGL4 reporter plasmid was constructed by subcloning the *IL-28B* promoter subfragment (nt −858 to +30). The combinations of two regulatory SNPs (rs72258881 or rs4803219) were introduced into the pGL4 vector (pGL4/WW, MW, WM, and MM). (B) Raji cells were co-transfected with pGL4 plasmids (0.05 g), and pGL4.74 control plasmid (0.05 g), and tested for firefly as well as renilla luciferase after LPS stimulation (3 μg/mL) for 4 h following IFN-α treatment (100 U/mL) for 16 h. These cells were seeded in a 96-well plate at 10^4 cells/well. The luciferase activities were normalized with renilla activities and data are presented as fold induction from activation of control vector. Bars indicate the means ± SD of triplicate determinations and the results are from one of three experiments. Statistical analyses are shown in table S2 to avoid complication. (C) For real-time PCR, the combinations of two regulatory SNPs (rs72258881 or rs4803219) were introduced into the pdCMV vector harboring a FLAG sequence (pdCMV/WW, MW, WM, and MM). (D) Jurkat cells were co-transfected with pdCMV plasmids (0.05 μg) and secreted alkaline phosphatase (SEAP) control plasmid (0.05 μg) and the expression levels were quantified using specific primer after LPS and IFN-α stimulation. The FLAG expression levels were normalized with SEAP activities and GAPDH as described in method section. Data are presented as fold induction from expression levels of pdCMV/WW. Bars indicate the means ± SD of triplicate determinations and the results are from one of three experiments. Statistical analyses are shown in table S3 to avoid complication.

doi:10.1371/journal.pone.0026620.g003

after IFN-α and LPS stimulation (Fig. 3D), suggesting that the length of TA repeat in the regulatory region of *IL-28B* could affect the regulation of *IL-28B* transcription.

Two intron SNPs located near the branch site of splicing

To determine the effect of the two iSNPs on pre-mRNA splicing, HeLa cells were transfected with wild type (WT), a construct with a double mutation of the iSNPs (d-iSNPs), or an antisense (AS) plasmid driven by the CMV promoter (Fig. 4A). The construct providing antisense transcription controlled by the CMV promoter was used to control for splicing defects (AS). Transcripts were analyzed by RT-PCR using primers in exon 1–2, 3–4, and 4–5. The RNA isolated from the WT and d-iSNPs yielded a single band using the three primer pairs. In contrast, longer amplicons were generated in cells expressing the antisense construct (Fig. 4B). The PCR products were sequenced to confirm the origin of the aberrant splicing events derived from the antisense construct (data not shown). The sequence analyses confirmed that PCR products from the WT and d-iSNPs were generated by normal splicing, suggesting that these two intron SNPs resulted in no splicing defects under these conditions.

No effect of nonsynonymous SNPs on IL-28B function

A nonsynonymous SNPs (rs8103142) located in the 3rd exon (Table 1 and Fig. 2D) led to the amino acid substitution $K^{74}R$ (Fig. 5A). Interestingly, the amino acid at this position is almost always arginine in homologous mammalian IFN-λs (e.g. human IL-28A, mouse IL-28A/B, and rhesus IL-28A/B). Then, the $K^{74}R$ substitution was expected to change IL-28B activity. The purified recombinant IL-28B protein (wild type) and the variant (ns-mut) were recognized by anti-IL-28B polyclonal antibody in a western blot assay (Fig. 5B). Based on spectrophotometric measurement of the protein concentration of the eluted fraction, it was calculated that at least 360 μg/mL of purified recombinant IL-28B protein (wild type and ns-mut) was obtained after purification. Flow-through liquid without recombinant protein was provided in the column preparing the sample of pcDNA3.1/AS (Fig. 5B). Molecular processing of IL-28B protein was confirmed to determine the precise N-terminal amino acid by peptide sequencer as the processing site of signal peptide was predicted by computer simulation (http://www.uniprot.org/uniprot/Q8IZI9). Then, the N-terminal sequence, VPVAR, was obtained (data not shown), suggesting that the simulation data was consistent with the form of physiological protein.

To evaluate the effect of nsSNPs on ISRE activity, three hepatoma cell lines (HuH7, HepG2, and HuSE2) expressing IL-28RI and IL-10R2 were transfected with pISRE-Luc and pGL4.74. These recombinant proteins were added to the supernatant (5 ng/mL each). As shown in Fig. 5C, ISRE activity of the ns-mut protein was similar to that of wild type protein in each cell line. IFN-α (100 U/mL), as a positive control of ISRE activity, showed a strong ISRE activity. These results suggested that the nonsynonymous mutation of rs8103142 did not affect IL-28B activity *in vitro*.

The genetic variation of TA repeats at the upstream of *IL-28B*

The reference sequence (RefSeq) of the human genome in the international database registers the TA repeat SNPs, rs72284729 or rs72258881, in the regulatory regions of *IL-28A* and *IL-28B*, respectively. The registered basal number of $(TA)_n$ is 8 in the regulatory region of *IL-28A* on the plus strand, whereas that of *IL-28B* is 13 on the minus strand encoding the gene (Table 2). From 20 Japanese healthy volunteers, genomic DNA was extracted to determine the actual $(TA)_n$ number located in the region of *IL-28A* or *IL-28B* by direct sequencing and, when direct sequencing chromatographs of $(TA)_n$ heterozygotes showed mixed patterns from the end of the TA repeat (Fig. S4), the mixed samples were subjected to cloning analysis. Interestingly, the $(TA)_n$ number in *IL-28A* was consistently different from dbSNP data, whereas that of *IL-28B* showed varying numbers along with SNPs data. The $(TA)_n$ range of *IL-28B* was from 10 to 18, and the most prevalent genotype was 12/12 (75%) in healthy Japanese volunteers.

To determine the functional significance of the TA indel, the regulatory region from −858 bp to +30 bp modifying the $(TA)_n$ number was cloned into the pGL4 reporter vector, transfected into HeLa cells, and assessed for firefly luciferase reporter gene

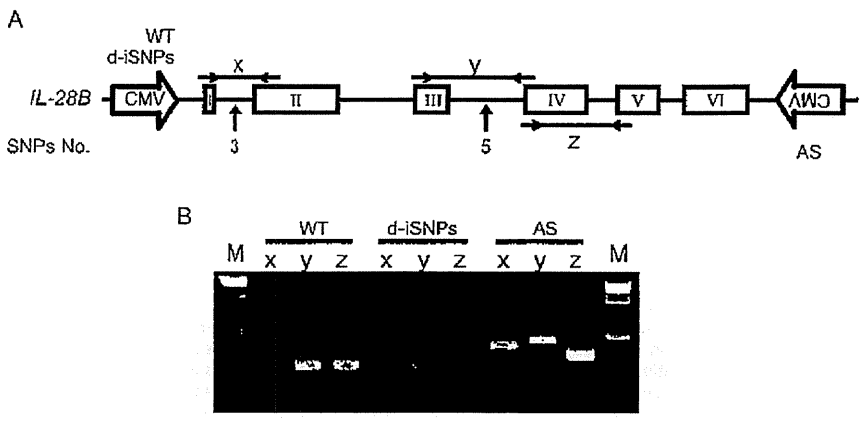

Figure 4. The determination of intron SNPs located near the branch site of splicing. (A) The expression plasmid of WT, d-iSNPs, or antisense (AS) derived from the CMV promoter was transfected into HeLa cells. Schematic of the WT, d-iSNPs, or AS used in the transfection experiments. PCR primers were designed to amplify products between exons. The effect of No. 3 and 5 SNPs (rs28416813 or rs11881222) on splicing were examined by amplicons x and y, respectively. The amplicon z was used for a splicing control. (B) Isolated RNAs were amplified by RT-PCR. The amplified products were checked by 2% agarose gel electrophoresis. The bands from the AS plasmid transcribing antisense represented abnormal splicing of mRNA as a control. Results shown are representative of three independent experiments.
doi:10.1371/journal.pone.0026620.g004

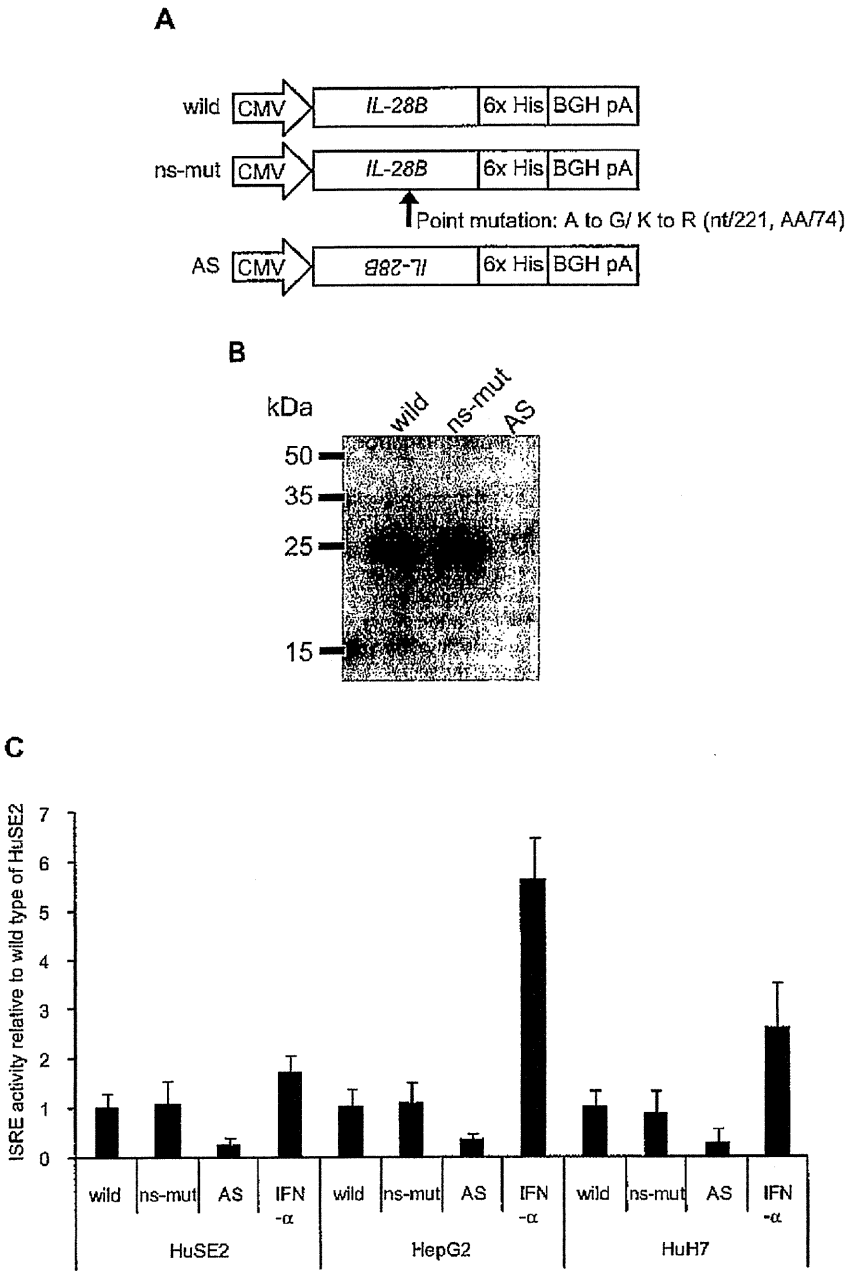

Figure 5. The purification and the activity of recombinant IL-28B with or without nsSNP. (A) The 6×His-tagged expression plasmid of wild type, ns-mut, or AS controlled by the CMV promoter was transfected into 293F cells. Schematics are the wild type, ns-mut and AS used in the transfection experiments. The procedure for recombinant protein purification is described in the materials and methods section. (B) The purified products were confirmed by immunoblotting using anti-IL28B antibody and the secondary antibody. The prepared proteins were loaded onto a 12% polyacrylamide gel. Bands corresponding to the expected molecular weight of IL-28B were observed in the wild type and ns-mut lanes. (C) For luciferase assay, HeLa cells were seeded into a 96-well plate at 10^4 cells/well and transfected with pISRE-Luc and pGL4.74 control vector before 16 h of IFN-α or IL-28B stimulation. Five ng/mL of IL-28B wild or ns-mut was added to the culture medium. Flow-though liquid from AS expression was used as a negative control. IFN-α (100 U/mL) was added for positive control of ISRE activity. The luciferase activities were normalized with Renilla activities and data are presented as fold induction from the basal promoter activation of the wild type. Bars indicate the means ± SD of triplicate determinations and the results are from one of three experiments.
doi:10.1371/journal.pone.0026620.g005

Table 2. The variations of TA repeat in *IL-28A* and *28B*.

		Location	
Gene	Data	rs72284792*[1]	rs72258881
IL-28A	RefSeq. (hg19)	$(TA)_6$	
	Cloning	$(TA)_6$	
IL-28B	RefSeq. (hg19)		$(TA)_{13}$
	Cloning		$(TA)_{10-18}$

*[1]The ID represents rs72258881, rs59702201, and rs67461793 because these three are located in the same genomic region, the TA repeat.
doi:10.1371/journal.pone.0026620.t002

expression (Fig. 6A). These cells were treated with 100 U/mL of IFN-α and 3 μg/mL of LPS. The results indicated that the variation in the $(TA)_n$ number at this polymorphic locus differentially regulates transcription. The transcriptional activation of the luciferase reporter gene was increased according to the $(TA)_n$ number (Fig. 6B).

Discussion

Four independent GWAS approaches have revealed the significant SNPs associated with response to PEG-IFNα/RBV therapy for CHC [12,13,14,19]. These significant SNPs were found around *IL-28B* but not *IL-28A*. The SNPs found in clinical studies to determine the outcome of HCV therapy were rs12979860 and rs8099917, because they showed the statistical significance in each study [12,13,14,19]. However, several SNPs around *IL-28B* were in strong LD (r^2>0.96) in JPT and CEU populations, although relatively low LD was predicted in the YRI population [16], and so it might be difficult to determine the most informative SNP [16]. These results suggest that any of the SNPs contained in this region could be of predictive value.

As reported in previous studies, transcription of *IL-28A/B* was upregulated in the TT genotype of rs8099917, which was associated with SVR [13,14,20], suggesting that the expression levels of *IL-28B* could be one of the key factors to clear HCV under PEG-IFNα/RBV therapy and could also affect spontaneous clearance of acute HCV infection [15]. To elucidate this question, we examined the function of the SNPs around the *IL-28B* gene to identify those SNPs affecting *IL-28B* expression. The new findings are as follows: 1) the gene structure of *IL-28B* comprised six exons in the several cell lines tested, although it was registered as having five exons in the CCDS database of NCBI. 2) The substitution of intron SNPs and non-synonymous SNPs in the *IL-28B* gene did not influence the expression levels or function. 3) Increased numbers of TA repeats in the promoter region of the *IL-28B* gene enhanced the transcription activity and expression level of the *IL-28B* gene. Because administration of IL-28B has been shown to have antiviral effects [21,22,23], lower expression of IL-28B might lead to a decrease in this effect.

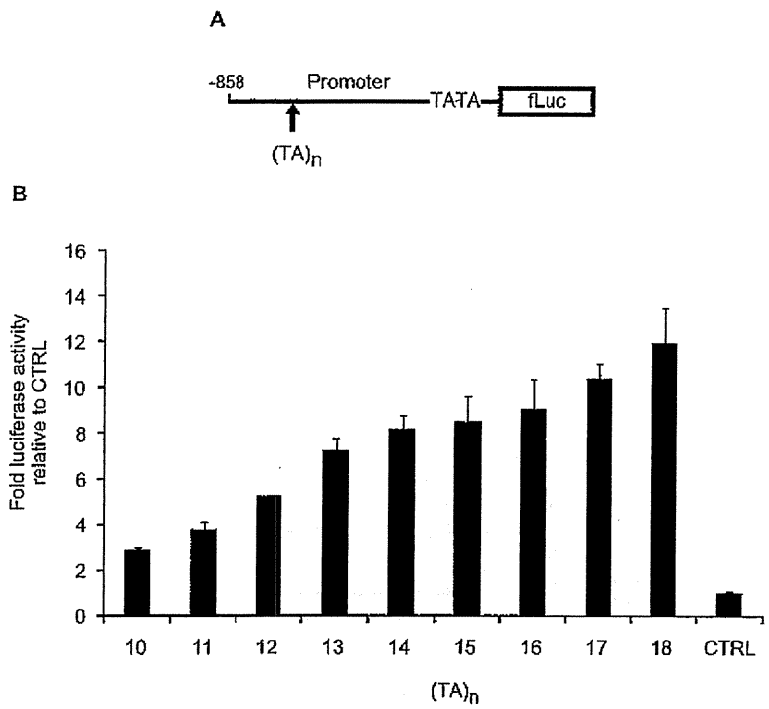

Figure 6. Luciferase assay of $(TA)_n$ number. (A) *IL-28B* promoter subfragment (nt −858 to +30) modifying $(TA)_n$ number from 10 to 18 was constructed in the pGL4 vector. (B) Raji cells were co-transfected with pGL4 plasmids (0.05 g), and pGL4.74 control plasmid (0.05 g), and tested for firefly as well as renilla luciferase after LPS stimulation (3 μg/mL) for 4 h following IFN-α treatment (100 U/mL) for 16 h. These cells were seeded into a 96-well plate at 10^4 cells/well. The luc activities were normalized with renilla activities and data are presented as fold induction from the activation of the control vector. Bars, the means ± SD of triplicate determinations and the results are from one of three experiments. Statistical analyses are shown in table S4 to avoid complication.
doi:10.1371/journal.pone.0026620.g006

The locations of two SNPs associated with response to HCV therapy, rs8099917 and rs12979860, are approximately 8 kb and 3 kb upstream of *IL-28B* gene, respectively. Because these SNPs, which showed the greatest statistical significance in the previous study, are located far from the *IL-28B* gene, another approach was required to determine the effect of the SNPs. In this study, broad $(TA)_n$ variations were observed in rs8099917 heterozygotes among CHC patients. Interestingly, a combination of TG and 11/12 genotype was strongly associated with NVR, whereas patients harboring the 12/13 genotype showed a virological response, regardless of the TG genotype (rs8099917). In clinical practice, genetic diagnosis using TA variation, following the primary classification of rs8099917 genotype, could improve the prediction of treatment response for CHC patients with the rs8099917 TG genotype. It is not clear whether the variation originates from genetic or epigenetic mechanisms. In addition, as the frequency of TA variation might be dependent on the particular population, further study will be needed to compare the frequency in several populations. A long TA repeat, over $(TA)_{13}$, was observed in healthy volunteers and showed potential for higher gene expression compared with under $(TA)_{13}$ constructs *in vitro*. It may be possible that spontaneous clearance of HCV infection and CHC patients are affected by this region because this also is dependent on *IL-28B* genotype [15,19]. In our speculation, the combination of both TA variation and the landmark SNPs, rs8099917 and rs12979860, might improve the prediction value. In addition, convenient diagnosis method to detect the TA variation like SNPs typing is needed since the present capillary techniques are relative complexity compared with SNPs typing.

In the international database, some SNPs ID are registered in the TA repeat region, located in the regulatory regions of the *IL-28A* and *IL-28B* gene, rs72284792 and rs7225881, respectively, whereas in our analysis separating *IL-28A* from *IL-28*, TA variation was detected only in the *IL-28B* region. SNP data often have been collected using next generation sequencing and based on short sequence reads. Unfortunately, the sequence similarity between *IL-28A* and *IL-28B* is over 90% from the CpG island to the region downstream of 3′-UTR. Alignment failure would occur for a high percentage of sequences when analyzed with software using general algorithms.

Effects of insertion/deletion (indel) polymorphism are known in the field of pharmacogenetic research. A polymorphism in the promoter of the uridine diphosphoglucuronosyl transferase 1A1 (*UGT 1A1*) gene has been shown to cause Crigler-Najjar syndrome types I and II and Gilbert syndrome, a benign form of unconjugated hyperbilirubinemia, and the occurrence of severe toxic events in irinotecan (known as CPT-11) administration [24,25,26]. The polymorphism consists of a $(TA)_n$ repeat in the 5′-promoter region [24,26,27], similar to that in this study. The range of repeat numbers is from $(TA)_5$ to $(TA)_8$ in the *UGT 1A1* gene [28]. The genetic disorder of the TA repeat length affects enzyme activity. The hepatic bilirubin *UGT 1A1* activity of individuals with Gilbert's syndrome is <30% of normal [29]. Irinotecan is used or under evaluation for a broad spectrum of solid tumors. Irinotecan pharmacokinetic parameters display a wide inter-patient variability and are involved in the genesis of toxic side effects [30,31,32,33]. Based on the polymorphism of the TA repeat, previous papers reported the association of irinotecan-induced severe toxicity with Gilbert's syndrome [34,35,36]. The value of genetic diagnosis of the *UGT1A1* polymorphisms prior to irinotecan chemotherapy has been corroborated in a previous study [37]. As similar characteristics were observed in the upstream region of *IL-28B*, the $(TA)_n$ repeat might be associated with disease progression as well as response to anti-HCV treatment.

In terms of epigenetic aspects, the TA variation of *IL-28B* was also suspected to be related to microsatellite instability, because a gap between the significant SNPs and TA variation was observed in this study. DNA mismatch repair (MMR) deficiency causes a high frequency of microsatellite instability (MSI-H), which is characterized by length alterations within simple repeated sequences, microsatellites. Lynch syndrome is primarily due to germline mutations in one of the DNA MMR genes, hMLH1 or hMSH2 [38]. MSI-H is also observed in <15% of colorectal, gastric and endometrial cancers, where it is associated with the hypermethylation of the promoter region of hMLH1 [39,40]. The diagnosis of MSI-H in cancers is therefore useful for identifying patients with Lynch syndrome and the efficacy of chemotherapy [41,42,43,44,45,46].

In conclusion, a (TA) dinucleotide repeat, rs72258881, located in the promoter region, was discovered by our functional studies of the proximal SNPs around *IL-28B*; the transcriptional activity of the promoter increased gradually in a $(TA)_n$ length-dependent manner. Combination diagnosis based on rs8099917 and rs72258881 might provide improved prediction because the $(TA)_n$ variation of *IL-28B* was observed but not that of *IL-28A*. The further study is needed to reveal the association with treatment response using clinical specimens of CHC. These findings suggest that the dinucleotide repeat could be associated with the transcriptional activity of *IL-28B* as well as constituting a predictor to improve prediction of the response to interferon-based HCV treatment.

Supporting Information

Figure S1 Sequence alignment of *IL-28A/B* cDNA retrieved from the database. The cDNA sequences of *IL-28A/B* were retrieved from the international database using accession number. The cDNA data reported by Sheppard et al. are AY129148 (*IL-28A*) and AY129149 (*IL-28B*) indicated with '_S' in the figure, and that of Kotenko et al. are AY184373 (*IL-28A*) and AY184374 (*IL-28B*) indicated with '_K'. Dashed boxes show the start codon predicted by computational analysis of the human genome reported by Sheppard et al. and Kotenko et al. The sequence alignment was calculated with Lasergene software (DNASTAR, Madison, WI).
(PDF)

Figure S2 Structural similarity between *IL-28A* and *IL-28B*. (A) Schematic of *IL-28A/B* gene location (UCSC genome browser). Boxes show the region representing high levels of structural similarity around *IL-28A/B*. (B) Modified schematic of structural similarity with a percentage. (C) Alignment between IL-28A and IL-28B from the CpG island to the region downstream of 3′-UTR. Homologous regions are shown by red characters. High levels of structural similarity were observed in CpG island, regulatory and gene region bypassing the in/del site.
(PDF)

Figure S3 Innate immune receptor expression related to IL-28B regulation. The relevant receptors for this study were confirmed by PCR using specific primers. (A) The mRNA expression of TLR4 was detected in cell lines, HeLa, Jurkat, MT-2, Raji, and PBMC. (B) For the study of cytokine-receptor association, the expression of IL-28RA and IL-10RB second receptor were examined using cDNA obtained from HuH7, HepG2, and HuSE2 cells. Samples without reverse transcriptase were prepared as a negative control in addition to the checking of genome contamination.
(PDF)

Figure S4 Direct sequencing analysis of TA repeat. In the first step to determine $(TA)_n$ genotypes, direct sequencing was

applied to amplicons of *IL-28A* or *28B* separated by gel electrophoresis. Homozygotes of TA repeat showed clear patterns and a high quality value in the bar above, whereas the patterns of heterozygotes were mixed because the length differed between alleles. The mixed patterns are shown in dashed boxes. These mixed products were cloned into the pGEM-Teasy vector to isolate and count the $(TA)_n$ number by sequencing of both alleles. (PDF)

Table S1
(DOC)

Table S2
(DOC)

Table S3
(DOC)

Table S4
(DOC)

Acknowledgments

We gratefully acknowledge Dr. Naoya Sakamoto for help with reporter vector (Tokyo Medical and Dental University). We also thank the following for their technical assistance: Dr. Shuko Murakami, Ms. Hatsue Naganuma, Ms. Kyoko Akita (Nagoya City University).

Author Contributions

Conceived and designed the experiments: MS YT MN TW MM. Performed the experiments: MS YT. Analyzed the data: MS YT. Contributed reagents/materials/analysis tools: MS YT MN TW MM. Wrote the paper: MS YT MN TW MM.

References

1. Kotenko SV, Gallagher G, Baurin VV, Lewis-Antes A, Shen M, et al. (2003) IFN-lambdas mediate antiviral protection through a distinct class II cytokine receptor complex. Nat Immunol 4: 69–77.
2. Sheppard P, Kindsvogel W, Xu W, Henderson K, Schlutsmeyer S, et al. (2003) IL-28, IL-29 and their class II cytokine receptor IL-28R. Nat Immunol 4: 63–68.
3. Mordstein M, Kochs G, Dumoutier L, Renauld JC, Paludan SR, et al. (2008) Interferon-lambda contributes to innate immunity of mice against influenza A virus but not against hepatotropic viruses. PLoS Pathog 4: e1000151.
4. Sommereyns C, Paul S, Staeheli P, Michiels T (2008) IFN-lambda (IFN-lambda) is expressed in a tissue-dependent fashion and primarily acts on epithelial cells in vivo. PLoS Pathog 4: e1000017.
5. Doyle SE, Schreckhise H, Khuu-Duong K, Henderson K, Rosler R, et al. (2006) Interleukin-29 uses a type 1 interferon-like program to promote antiviral responses in human hepatocytes. Hepatology 44: 896–906.
6. Marcello T, Grakoui A, Barba-Spaeth G, Machlin ES, Kotenko SV, et al. (2006) Interferons alpha and lambda inhibit hepatitis C virus replication with distinct signal transduction and gene regulation kinetics. Gastroenterology 131: 1887–1898.
7. Zhou Z, Hamming OJ, Ank N, Paludan SR, Nielsen AL, et al. (2007) Type III interferon (IFN) induces a type I IFN-like response in a restricted subset of cells through signaling pathways involving both the Jak-STAT pathway and the mitogen-activated protein kinases. J Virol 81: 7749–7758.
8. Bartlett NW, Buttigieg K, Kotenko SV, Smith GL (2005) Murine interferon lambdas (type III interferons) exhibit potent antiviral activity in vivo in a poxvirus infection model. J Gen Virol 86: 1589–1596.
9. Brand S, Zitzmann K, Dambacher J, Beigel F, Olszak T, et al. (2005) SOCS-1 inhibits expression of the antiviral proteins 2',5'-OAS and MxA induced by the novel interferon-lambdas IL-28A and IL-29. Biochem Biophys Res Commun 331: 543–548.
10. Robek MD, Boyd BS, Chisari FV (2005) Lambda interferon inhibits hepatitis B and C virus replication. J Virol 79: 3851–3854.
11. Zhu H, Butera M, Nelson DR, Liu C (2005) Novel type I interferon IL-28A suppresses hepatitis C viral RNA replication. Virol J 2: 80.
12. Ge D, Fellay J, Thompson AJ, Simon JS, Shianna KV, et al. (2009) Genetic variation in IL28B predicts hepatitis C treatment-induced viral clearance. Nature 461: 399–401.
13. Suppiah V, Moldovan M, Ahlenstiel G, Berg T, Weltman M, et al. (2009) IL28B is associated with response to chronic hepatitis C interferon-alpha and ribavirin therapy. Nat Genet 41: 1100–1104.
14. Tanaka Y, Nishida N, Sugiyama M, Kurosaki M, Matsuura K, et al. (2009) Genome-wide association of IL28B with response to pegylated interferon-alpha and ribavirin therapy for chronic hepatitis C. Nat Genet 41: 1105–1109.
15. Thomas DL, Thio CL, Martin MP, Qi Y, Ge D, et al. (2009) Genetic variation in IL28B and spontaneous clearance of hepatitis C virus. Nature 461: 798–801.
16. Tanaka Y, Nishida N, Sugiyama M, Tokunaga K, Mizokami M (2010) lambda-Interferons and the single nucleotide polymorphisms: A milestone to tailor-made therapy for chronic hepatitis C. Hepatol Res 40: 449–460.
17. Siren J, Pirhonen J, Julkunen I, Matikainen S (2005) IFN-alpha regulates TLR-dependent gene expression of IFN-alpha, IFN-beta, IL-28, and IL-29. J Immunol 174: 1932–1937.
18. Livak KJ, Schmittgen TD (2001) Analysis of relative gene expression data using real-time quantitative PCR and the 2(-Delta Delta C(T)) Method. Methods 25: 402–408.
19. Rauch A, Kutalik Z, Descombes P, Cai T, Di Iulio J, et al. (2010) Genetic variation in IL28B is associated with chronic hepatitis C and treatment failure: a genome-wide association study. Gastroenterology. pp 138–1338–1345, 1345 e1331–1337.
20. Fukuhara T, Taketomi A, Motomura T, Okano S, Ninomiya A, et al. (2010) Variants in IL28B in liver recipients and donors correlate with response to peg-interferon and ribavirin therapy for recurrent hepatitis C. Gastroenterology. pp 139–1577–1585, 1585 e1571–1573.
21. Ank N, Iversen MB, Bartholdy C, Staeheli P, Hartmann R, et al. (2008) An important role for type III interferon (IFN-lambda/IL-28) in TLR-induced antiviral activity. J Immunol 180: 2474–2485.
22. Ank N, West H, Bartholdy C, Eriksson K, Thomsen AR, et al. (2006) Lambda interferon (IFN-lambda), a type III IFN, is induced by viruses and IFNs and displays potent antiviral activity against select virus infections in vivo. J Virol 80: 4501–4509.
23. Contoli M, Message SD, Laza-Stanca V, Edwards MR, Wark PA, et al. (2006) Role of deficient type III interferon-lambda production in asthma exacerbations. Nat Med 12: 1023–1026.
24. Bosma PJ, Chowdhury JR, Bakker C, Gantla S, de Boer A, et al. (1995) The genetic basis of the reduced expression of bilirubin UDP-glucuronosyltransferase 1 in Gilbert's syndrome. N Engl J Med 333: 1171–1175.
25. Monaghan G, Ryan M, Seddon R, Hume R, Burchell B (1996) Genetic variation in bilirubin UPD-glucuronosyltransferase gene promoter and Gilbert's syndrome. Lancet 347: 578–581.
26. Raijmakers MT, Jansen PL, Steegers EA, Peters WH (2000) Association of human liver bilirubin UDP-glucuronyltransferase activity with a polymorphism in the promoter region of the UGT1A1 gene. J Hepatol 33: 348–351.
27. Sato H, Adachi Y, Koiwai O (1996) The genetic basis of Gilbert's syndrome. Lancet 347: 557–558.
28. Beutler E, Gelbart T, Demina A (1998) Racial variability in the UDP-glucuronosyltransferase 1 (UGT1A1) promoter: a balanced polymorphism for regulation of bilirubin metabolism? Proc Natl Acad Sci U S A 95: 8170–8174.
29. Yamamoto K, Sato H, Fujiyama Y, Doida Y, Bamba T (1998) Contribution of two missense mutations (G71R and Y486D) of the bilirubin UDP glycosyltransferase (UGT1A1) gene to phenotypes of Gilbert's syndrome and Crigler-Najjar syndrome type II. Biochim Biophys Acta 1406: 267–273.
30. Gupta E, Lestingi TM, Mick R, Ramirez J, Vokes EE, et al. (1994) Metabolic fate of irinotecan in humans: correlation of glucuronidation with diarrhea. Cancer Res 54: 3723–3725.
31. Gupta E, Mick R, Ramirez J, Wang X, Lestingi TM, et al. (1997) Pharmacokinetic and pharmacodynamic evaluation of the topoisomerase inhibitor irinotecan in cancer patients. J Clin Oncol 15: 1502–1510.
32. Rowinsky EK, Grochow LB, Ettinger DS, Sartorius SE, Lubejko BG, et al. (1994) Phase I and pharmacological study of the novel topoisomerase I inhibitor 7-ethyl-10-[4-(1-piperidino)-1-piperidino]carbonyloxycamptothecin (CPT-11) administered as a ninety-minute infusion every 3 weeks. Cancer Res 54: 427–436.
33. Iyer L, King CD, Whitington PF, Green MD, Roy SK, et al. (1998) Genetic predisposition to the metabolism of irinotecan (CPT-11). Role of uridine diphosphate glucuronosyltransferase isoform 1A1 in the glucuronidation of its active metabolite (SN-38) in human liver microsomes. J Clin Invest 101: 847–854.
34. Sugatani J, Yamakawa K, Yoshinari K, Machida T, Takagi H, et al. (2002) Identification of a defect in the UGT1A1 gene promoter and its association with hyperbilirubinemia. Biochem Biophys Res Commun 292: 492–497.
35. Iyanagi T, Emi Y, Ikushiro S (1998) Biochemical and molecular aspects of genetic disorders of bilirubin metabolism. Biochim Biophys Acta 1407: 173–184.
36. Wasserman E, Myara A, Lokiec F, Goldwasser F, Trivin F, et al. (1997) Severe CPT-11 toxicity in patients with Gilbert's syndrome: two case reports. Ann Oncol 8: 1049–1051.
37. Sadee W, Dai Z (2005) Pharmacogenetics/genomics and personalized medicine. Hum Mol Genet 14 Spec No. 2: R207-214.
38. Modrich P (1994) Mismatch repair, genetic stability, and cancer. Science 266: 1959–1960.
39. Lengauer C, Kinzler KW, Vogelstein B (1997) DNA methylation and genetic instability in colorectal cancer cells. Proc Natl Acad Sci U S A 94: 2545–2550.

40. Lengauer C, Kinzler KW, Vogelstein B (1997) Genetic instability in colorectal cancers. Nature 386: 623–627.
41. Kim GP, Colangelo LH, Paik S, O'Connell MJ, Kirsch IR, et al. (2007) Predictive value of microsatellite instability-high remains controversial. J Clin Oncol 25: 4857; author reply 4857–4858.
42. Elsaleh H, Joseph D, Grieu F, Zeps N, Spry N, et al. (2000) Association of tumour site and sex with survival benefit from adjuvant chemotherapy in colorectal cancer. Lancet 355: 1745–1750.
43. Gryfe R, Kim H, Hsieh ET, Aronson MD, Holowaty EJ, et al. (2000) Tumor microsatellite instability and clinical outcome in young patients with colorectal cancer. N Engl J Med 342: 69–77.
44. Ribic CM, Sargent DJ, Moore MJ, Thibodeau SN, French AJ, et al. (2003) Tumor microsatellite-instability status as a predictor of benefit from fluorouracil-based adjuvant chemotherapy for colon cancer. N Engl J Med 349: 247–257.
45. Popat S, Hubner R, Houlston RS (2005) Systematic review of microsatellite instability and colorectal cancer prognosis. J Clin Oncol 23: 609–618.
46. Sinicrope FA, Rego RL, Halling KC, Foster N, Sargent DJ, et al. (2006) Prognostic impact of microsatellite instability and DNA ploidy in human colon carcinoma patients. Gastroenterology 131: 729–737.

Hepatology Research

Hepatology Research 2011; 41: 936–945 doi: 10.1111/j.1872-034X.2011.00859.x

Original Article

Easy-to-use phylogenetic analysis system for hepatitis B virus infection

Masaya Sugiyama,[1,2]* Ayano Inui,[3] Tadasu Shin-I,[1] Haruki Komatsu,[3] Motokazu Mukaide,[1,4] Naohiko Masaki,[1] Kazumoto Murata,[1] Kiyoaki Ito,[1] Makoto Nakanishi,[2] Tomoo Fujisawa[3] and Masashi Mizokami[1]

[1]*The Research Center for Hepatitis and Immunology, National Center for Global Health and Medicine, Ichikawa,* [2]*Department of Biochemistry and Cell Biology, Nagoya City University Graduate School of Medical Sciences, Nagoya,* [3]*Department of Pediatrics, Eastern Yokohama Hospital, Yokohama, and* [4]*SRL, Inc. Tokyo, Japan*

Aim: The molecular phylogenetic analysis has been broadly applied to clinical and virological study. However, the appropriate settings and application of calculation parameters are difficult for non-specialists of molecular genetics. In the present study, the phylogenetic analysis tool was developed for the easy determination of genotypes and transmission route.

Methods: A total of 23 patients of 10 families infected with hepatitis B virus (HBV) were enrolled and expected to undergo intrafamilial transmission. The extracted HBV DNA were amplified and sequenced in a region of the S gene.

Results: The software to automatically classify query sequence was constructed and installed on the Hepatitis Virus Database (HVDB). Reference sequences were retrieved from HVDB, which contained major genotypes from A to H. Multiple-alignments using CLUSTAL W were performed before the genetic distance matrix was calculated with the six-parameter method. The phylogenetic tree was output by the neighbor-joining method. User interface using WWW-browser was also developed for intuitive control. This system was named as the easy-to-use phylogenetic analysis system (E-PAS). Twenty-three sera of 10 families were analyzed to evaluate E-PAS. The queries obtained from nine families were genotype C and were located in one cluster per family. However, one patient of a family was classified into the cluster different from her family, suggesting that E-PAS detected the sample distinct from that of her family on the transmission route.

Conclusions: The E-PAS to output phylogenetic tree was developed since requisite material was sequence data only. E-PAS could expand to determine HBV genotypes as well as transmission routes.

Key words: database, genotype, hepatitis B virus, intrafamilial transmission, phylogenetic analysis

INTRODUCTION

HEPATITIS B VIRUS (HBV) infects approximately 350 million people worldwide. Chronic HBV infection causes liver cirrhosis and liver cancer. In Japan, chronic hepatitis B patients are estimated to be approximately one million.[1] As HBV has high infectivity, almost all advanced countries have launched the universal infant immunization program against HBV. The patients with HB antigen seropositive, fulminant hepatitis and HCC have substantially declined in these countries.[2,3] The current immunization strategy represents favorable effects to prevent the HBV transmission. In countries without the universal vaccination program, however, substantial intrafamilial transmission and horizontal transmission have been reported.[4] In Japan, only high-risk infants born to chronic HBV-infected mothers have been given the HBV vaccine according to a selective vaccination policy of Japanese governments since 1986. This strategy has led to successful reduction of HBV carrier infants[5] since the major route of transmission has been perinatal transmission,[6,7] and horizontal transmission in early childhood has occurred as a result of close family contact.[8–10] However, the main

Correspondence: Dr Masashi Mizokami, The Research Center for Hepatitis and Immunology, National Center for Global Health and Medicine, 1-7-1, Kohnodai, Ichikawa 272-8516, Japan. Email: mmizokami@hospk.ncgm.go.jp
*JSPS Research Fellow.
Received 14 April 2011; revision 13 June 2011; accepted 15 June 2011.

route of acute hepatitis B in adult is sexual transmission in countries without a universal vaccination program.

Hepatitis B virus genotypes are identified worldwide and classified into at least eight genotypes (A–H) on the basis of a divergence of 8% or more of the entire nucleotide sequences.[1,11–13] In a Japanese population of chronic hepatitis B, the distribution of major HBV genotypes (HBV/A, B, C, and D) was reported to be 1.7%, 12.2%, 84.7%, and 0.4% respectively.[14] However, the prevalence of HBV/A increased to approximately 40% in acute HBV infection, and 4.3% in chronic HBV infection in Japan.[15] The main transmission routes of HBV/A are a contact among men who have sex with men as well as among members of a heterosexual population.[16–19] The expansion of HBV infection has been led by the sexual transmission of HBV/A since little infection by contaminated medical materials has recently been reported in Japan.

As previously reported, phylogenetic analyses based on virus genome revealed the transmission route.[20] The identification of the transmission route provides beneficial information for epidemiologic study and healthcare reform. Although phylogenetic analysis is gradually known in this field, the handlings of the data are difficult to achieve for researchers who are not familiar with genetic analysis. In this study, we have developed a novel computing system to output phylogenetic trees automatically when users simply input their sequence data. The result from this system also shows the type of transmission route such as intrafamilial (mother-to-child, father-to-child, or child-to-child) or horizontal in the general population. For this purpose, sera collected from 10 families with possible intrafamilial transmission were used to reveal their accurate transmission route.

METHODS

Patients

TEN FAMILIES CONSISTING of 23 patients being inactive carriers or having chronic hepatitis B were enrolled in this study after 32 individuals of 10 families

Table 1 Characteristics of intrafamilial transmission cases

Family	Feature	Age	Sex	HBV DNA (Log copies/mL)	Status 1	Status 2	ID
FM1	C	11	F	>9	eAg +	IC	1
	Mo	40	F	8.7	eAg +	IC	2
FM2	C	7	M	>9	eAg +	IC	3
	Mo/S1	41	F	8.6	eAg +	CH	4
	S2	27	F	<2.6	eAb +	IC	5
	S3	30	F	3	eAb +	IC	6
FM3	C	3	F	>9	eAg +	IC	7
	Mo	37	F	>9	eAg +	IC	8
FM4	C1	15	M	>9	eAg +	IC	9
	C2	20	F	>9	eAg +	IC	10
	Mo	47	F	>9	eAg +	IC	11
FM5	C	15	M	5.9	eAb +	IC	12
	Fa	46	M	4.2	eAb +	IC	13
FM6	C	12	M	>9	eAg +	CH	14
	Mo	36	F	>9	eAg +	CH	15
FM7	C	2	F	2.8	eAb +	IC	16
	Mo	33	F	>9	eAg +	IC	17
FM8	C	2	M	>9	eAg +	IC	18
	Mo	41	F	>9	eAg +	IC	19
FM9	C	7	M	3.5	eAb +	IC	20
	Mo	39	F	>9	eAg +	CH	21
FM10	C1	4	M	>9	eAg +	CH	22
	C2	2	F	<2.6	eAb +	IC	23

All patients were hepatitis B surface antigen (HBsAg) positive. Feature: C, children; Mo, mother; Fa, father; S, sister. Sex: M, male; F, female. Status1: Status of HB antigen or antibody except for HbsAg. Status2: IC, inactive carrier; CH, chronic hapatitis. ID 4, 5, 6 are sister and ID 4 is mother of ID 3. ID 22 and 23 are brother and sister.

were tested on HB markers (Table 1). All patients were hepatitis B surface antigen (HBsAg) positive, and the family cases had a possibility of intrafamilial transmission. The histories of familial clustering of HBV infection and hepatitis B vaccination were recorded. The serum samples obtained from all patients were tested for hepatitis B surface antigen (HBsAg), hepatitis B surface antibody (anti-HBs), and hepatitis B core antibody (anti-HBc). Four sera of chronic hepatitis B patients were collected for operation-checks of the developed system before a trial of 23 samples. Serum samples were divided into aliquots and kept at −80 °C until testing. The study protocol conformed to the 1975 declaration of Helsinki and was approved by the ethics committees of the respective institutions. Every patient or his/her next of kin gave informed consent to the purpose of the study. Consent of children for participating in the study was filled by their parents.

Serological testing

Their sera were tested for alanine aminotransferase (ALT), and hepatitis B e antigen (HBeAg) and hepatitis B s antigen (HBsAg), as well as antibodies to HBeAg (anti-HBe) and HBsAg (anti-HBs) (Dinabot, Tokyo, Japan). Antibodies to HBcAg (anti-HBc) were tested by ARCHITECT (Abbott Japan, Tokyo, Japan). The inactive carrier state was defined by the presence of HBV surface antigen (HBsAg) with normal ALT levels over 1 year (examined at least four times at 3-month intervals). Chronic hepatitis was defined by elevated ALT levels (>1.5 times the upper limit of normal [35 IU/L]) persisting over 6 months (with at least three bimonthly tests). HBV DNA levels in sera were quantitated with a commercial kit (Taqman Real-time polymerase chain reaction [PCR] or Amplicor HBV Monitor; Roche Diagnostics, Basel, Switzerland) with a detection range from 2.6 to 9 log copies/mL.

Viral DNA extraction

HBV DNA was extracted from 200 μL of serum using QIAamp DNA Blood Mini Kit (Qiagen, Valencia, CA, USA) according to manufacturer's instruction. The extracted DNA was used for amplification and direct sequencing of S gene as described below.

HBV DNA sequencing

The target of S gene (255 bp, nucleotide positions 458–712) was amplified by nested PCR and sequenced to detect in high sensitivity. The forward primers of S gene were HBS/F2, 5′- AGGTATGTTGCCCGTTTGTC -3′ for the outer set and HBS/F1, 5′- GTATGTTGCCCGTTT GTCCT -3′ for the inner set. The reverse primers of the gene were HBS/R2, 5′- AAAGCCCTACGAACCACTGA −3′ for the outer set and HBS/R1, 5′- AAGCCCTACG AACCACTGAA-3′ for the inner set. Nested PCRs were performed with these primers for 35 cycles (95 °C, 15 s; 58 °C, 30 s; 72 °C, 30 s) in 1st and 2nd PCR using Veriti (Applied Biosystems, Foster City, CA, USA). The PCR products were sequenced on both strands with the BigDye Terminator V3.1 cycle sequencing kit (Applied Biosystems) with the same primers used for the 2nd PCR. The sequencing products were analyzed with an ABI 3130xl DNA analyzer (Applied Biosystems). The obtained sequences were aligned with GenBank sequences corresponding to HBV genotypes.

Database and the system for phylogenetic analysis

The determination of transmission routes using phylogenetic analyses is considered based on age difference, mutation rate, clinical background, and the amplicon size between queries. The determination of non-intrafamilial transmission between queries was performed using a significance level of $P < 10^{-99}$. The criterion was calculated by the simulation of random sampling from Hepatitis Virus Database (HVDB) and the genetic factors described above. The presently developed system, the easy-to-use phylogenetic analysis system (E-PAS) for the determination of genotypes and/or transmission route is implemented in the account mode of the HVDB (http://s2as02.genes.nig.ac.jp). We recommend that researchers contact the web master before use.

Table 2 Reference data for the analysis of transmission root

Genotype	Country	Number of references
A	Foreign	2
B	Japan	24
C	Japan	64
D	Japan	1
E	Foreign	1
F	Foreign	1
G	Foreign	1
H	Japan	3

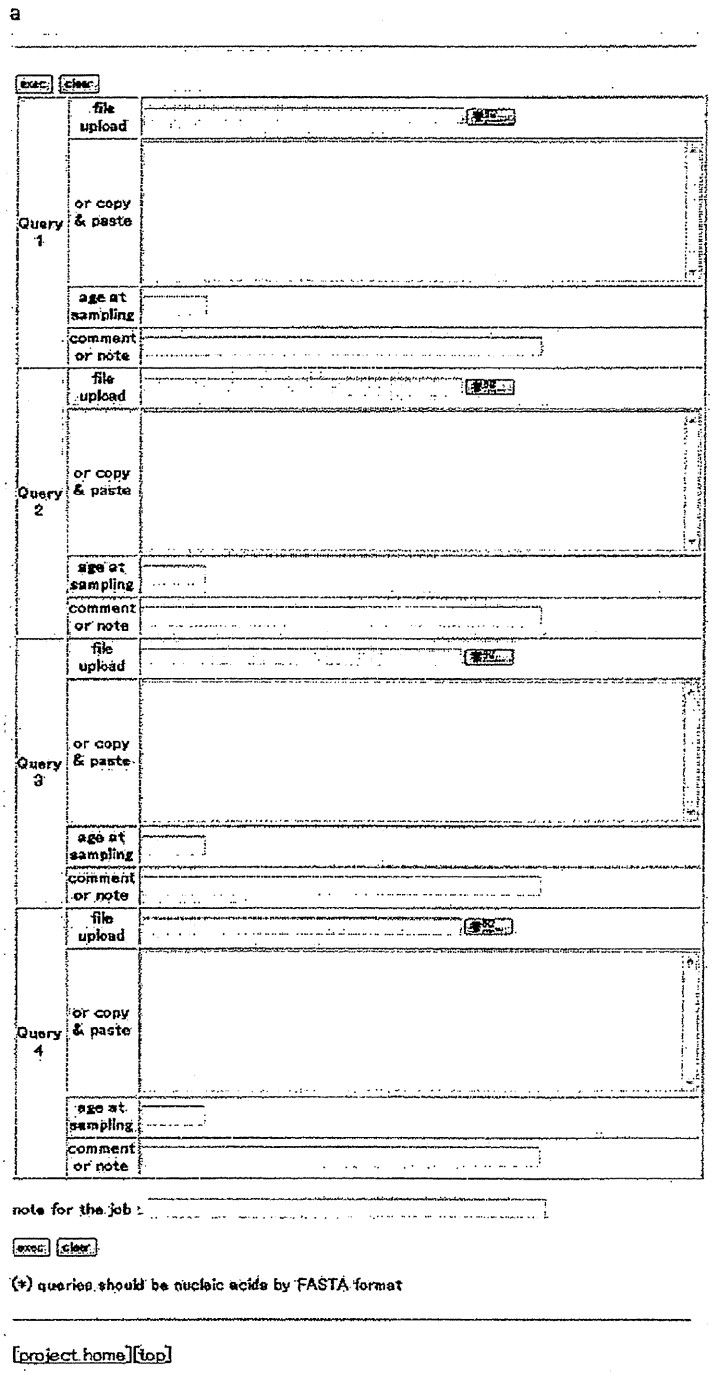

Figure 1 WWW-based user interface. To avoid bias such as age and selective pressure of antiviral treatment, adjustment parameters are prepared to obtain appropriate results. (a) The input field of query sequences and patient's age when serum was collected is shown. (b) The upper field configures masked sites for the elimination of drug-resistant sites. The lower field is a mutation rate of hepatitis B virus (HBV).

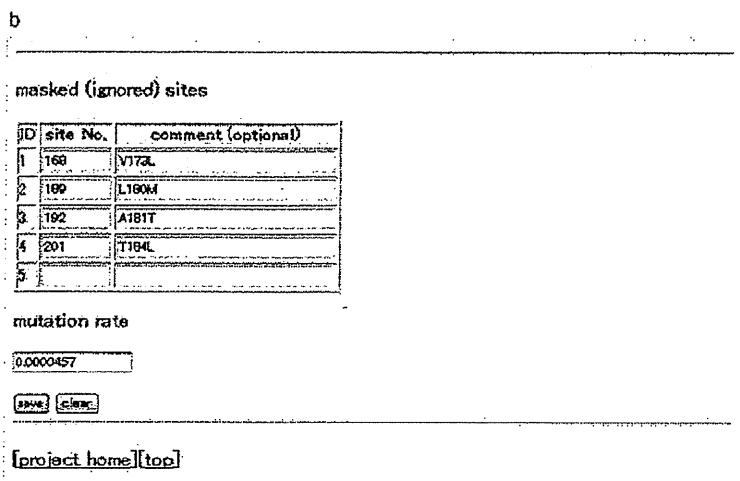

Figure 1 *Continued.*

RESULTS

Preparation of reference data

A DATASET OF all HBV S gene sequences that contain sequence variations in Japanese patients was retrieved from the HVDB[21] for reference sequences to classify suspicious samples of intrafamilial transmission. A representative sequence was selected among the same sequences in a cluster to optimize phylogenetic analysis. Full annotations of all sequences were also extracted from HVDB. The data of major genotypes were registered into the system. The results of the dataset were shown in Table 2.

Calculation for the classification of new sequences

New sequences input in query columns were calculated and then classified by the following process (Fig. 1a). The query sequences were added to the reference database described above, and the overall sequences were multiple-aligned by CLUSTAL W[22]. More precise alignment than direct alignment among queries was obtained regardless of the sequence quality of queries. Then, the genetic distance matrix was calculated from the alignment with the six-parameter method,[23] using only the sites shared by all the sequences. Finally the phylogenetic tree was constructed from the matrix using the neighbor-joining method,[24] which showed the relation among the queries, between query and published entries. The above calculation was conducted without using nucleotide positions of drug-induced resistant mutations to avoid selective pressure of antiviral treatment (Fig. 1b). As shown in Figure 1b, the mutation site of Lamivudin, Adefovir diproxil, and Entecavir resistance were masked in the present study along with the previous study.[25,26] We have estimated the substitution rate for HBV to be 4.57×10^{-5} per site per year.[27] In addition, the adjustment of age factor was calculated in consideration of genetic distance between queries for precise phylogenetic analysis (Fig. 1a). The distribution of nucleotide differences could be generally approximated by Poisson distribution and its average difference site number in the PCR amplicon of this study was 4.67 bases. The probability that two independent samples had the same sequence by chance was estimated to be less than 1%, and then the false positive data were seldom output in the intrafamilial transmission case. This system showed a sensitivity of 100% by calculating independent data retrieved from Osiowy *et al.*[28] The paper provided sequence data of a 25-year period obtained from eight asymptomatic carriers of the HBV genotype B in 1979 and 2004. For the calculation of the specificity, random sampling was performed using HVDB data. The specificity of this system was 98.6% by sampling 72 data.

Users interface

We also developed a WWW-based user interface to conduct the analysis easily. Researchers get two types of results in one analysis after they upload two or more query sequences through WWW browsers. One is a report of nucleotide difference number between

queries. This shows an indication of whether queries are similar enough or not. The other is a phylogenetic tree that shows the relation among queries and reference data.

Determination of transmission route in family cases

Four independent samples of chronic hepatitis B obtained from our hospital were tested before the analysis of suspicious intrafamilial transmission cases. Each of these four sequences was classified into distinct cluster (data not shown). As the E-PAS worked well, the analysis of suspicious intrafamilial transmission cases was examined to reveal whether two (or more) sequences obtained from a family were from intrafamilial transmission or not. The analysis was carried out by the process described above. The queries in the multiple alignments were compared between queries to count different nucleotide sites. Then, the comparison is done using the high-quality regions of the queries by ignoring ambiguous base ("N" base) sites. If three or more queries of a family were entered in the system, the comparison was calculated for each pair of queries. Table 1 shows characteristics of patients

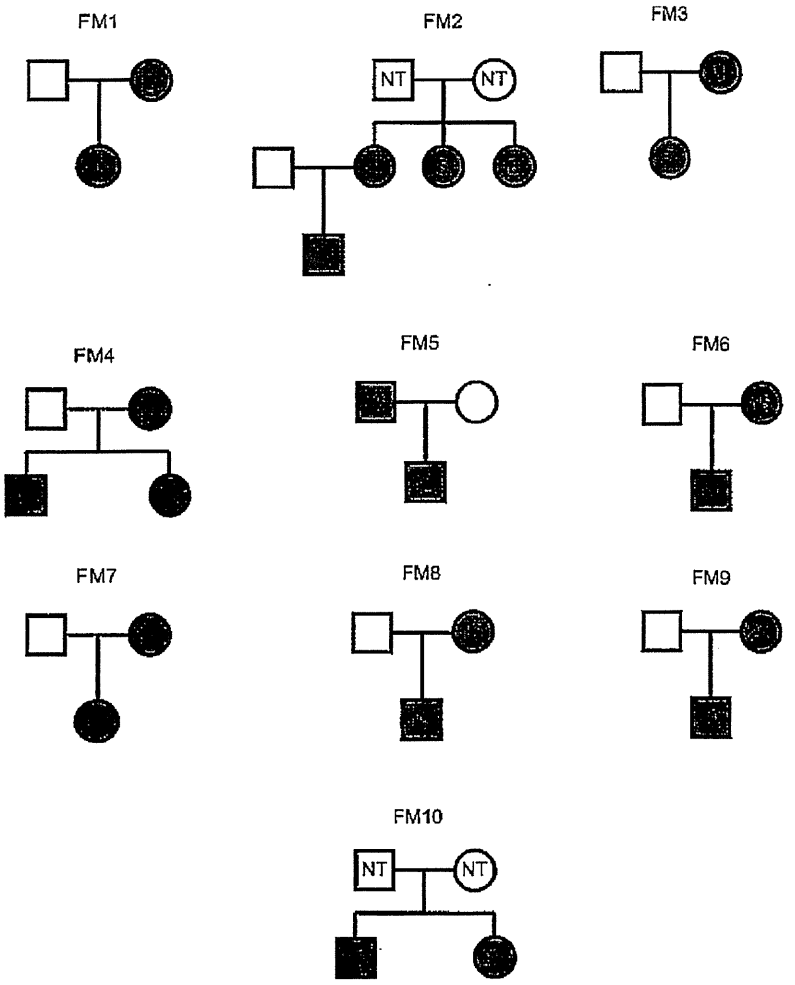

Figure 2 Family trees for 10 families with clustering hepatitis B virus (HBV) infection. Gray color indicates HBsAg positive, and white color indicates hepatitis B surface antigen (HBsAg) negative. Patients without HB antigen information are described as not tested (NT). Squares indicates male sex, circles indicates female sex.

Japanese HBV S gene classification results (user:msugiyam)

job : 20110731183753

comment : FM2

query	definition	age	nearest public entry				difference between queries								nearest cluster
			ID	subtype	overlap len	mismatch	overlap len	probe0		probe1		probe2		probe3	
								N-diff	Prob	N-diff	Prob	N-diff	Prob	N-diff	Prob
probe0	Child	7	AB246345	C	250	2	244	0	1	0	1	0	1	4	0.000000e+00	AB246345
probe1	Mother, Sister1	41	AB246345	C	249	1		0	1	0	1	0	1	4	0.000000e+00	AB246345, probe0
probe2	Sister2	27	AB246345	C	248	0		0	1	0	1	0	1	4	0.000000e+00	AB246345, probe0, probe1
probe3	Sister3	30	AB222735	C	246	2		4	0.000000e+00	4	0.000000e+00	4	0.000000e+00	0	1	AB247916, AB222735

Figure 3 WWW-based user interface and the results of the matrix calculation by the software. The queries registered on the system were multi-aligned and analyzed for the calculation of mismatched nucleotides between the members of the family. This figure shows a representative result using FM2 data. The definition column presents sample information. The age column shows the point when their sera was collected. The nearest public entry shows the data locating near the query and displays the genotype, the length of query, and mismatched nucleotides compared with the nearest reference entry. The column of the difference between queries represents the mismatched nucleotides between the queries. The N-diff column shows the mismatched nucleotides between the queries. The probability value of the difference between two queries displays the prob column.

infected with HBV. These 10 families were analyzed to determine the transmission route using the present system. Predictably, two or three sequence data obtained from one family were classified into one cluster except for FM2 case (data not shown), and then the transmission routes of these nine families were intrafamilial as was expected.

A case of multiple transmission routes in a family

Interestingly, the result of FM2 case was different from the others. As shown in Table 1 and Figure 2, the family consisted of four carriers (three sisters and one of their sons). The number of nucleotide differences was calculated after the multiple-alignment by CLUSTAL W. Sample ID 6 (sister 3, S3) showed four mismatched nucleotides compared with the other members in the family (see the column of difference between queries in Fig. 3), and then the phylogenetic tree was described using E-PAS in HVDB. As shown in Figure 4, the sequence of ID 6 was classified into the cluster far from the other member, suggesting that ID 6 was infected with a different HBV clone from the other member. The probability value (abbreviated as Prob in Fig. 3) of intrafamilial transmission between two queries is displayed in the browser.

DISCUSSION

WE HAVE DEVELOPED an easy-to-use system for the calculation of phylogenetic analysis. The present system (E-PAS) was constructed for non-specialist users of genetics as well as specialists and would provide the appropriate results with several adjusted parameters by just preparing sequence data. Therefore, this system is recommended to users who want to easily investigate transmission routes of samples. In the present study, we have applied the E-PAS to the determination of transmission routes in families. Almost all of the family-cases showed intrafamilial transmission because the queries belonging to one family were classified in same cluster or a neighboring position. In the analysis between families, these queries certainly were located in the distinct cluster. One patient (sample ID 6) showed quite different sequences from the other members of her family. We did not determine whether her transmission route was vertical or horizontal as data of her parents on HBV infection were not provided. If both parents were HBV carriers, the different sequences could be detectable among ID 4, 5, and 6 as an intrafamilial transmission from father or mother to child, or she was infected by a vertical transmission from non-familial member.

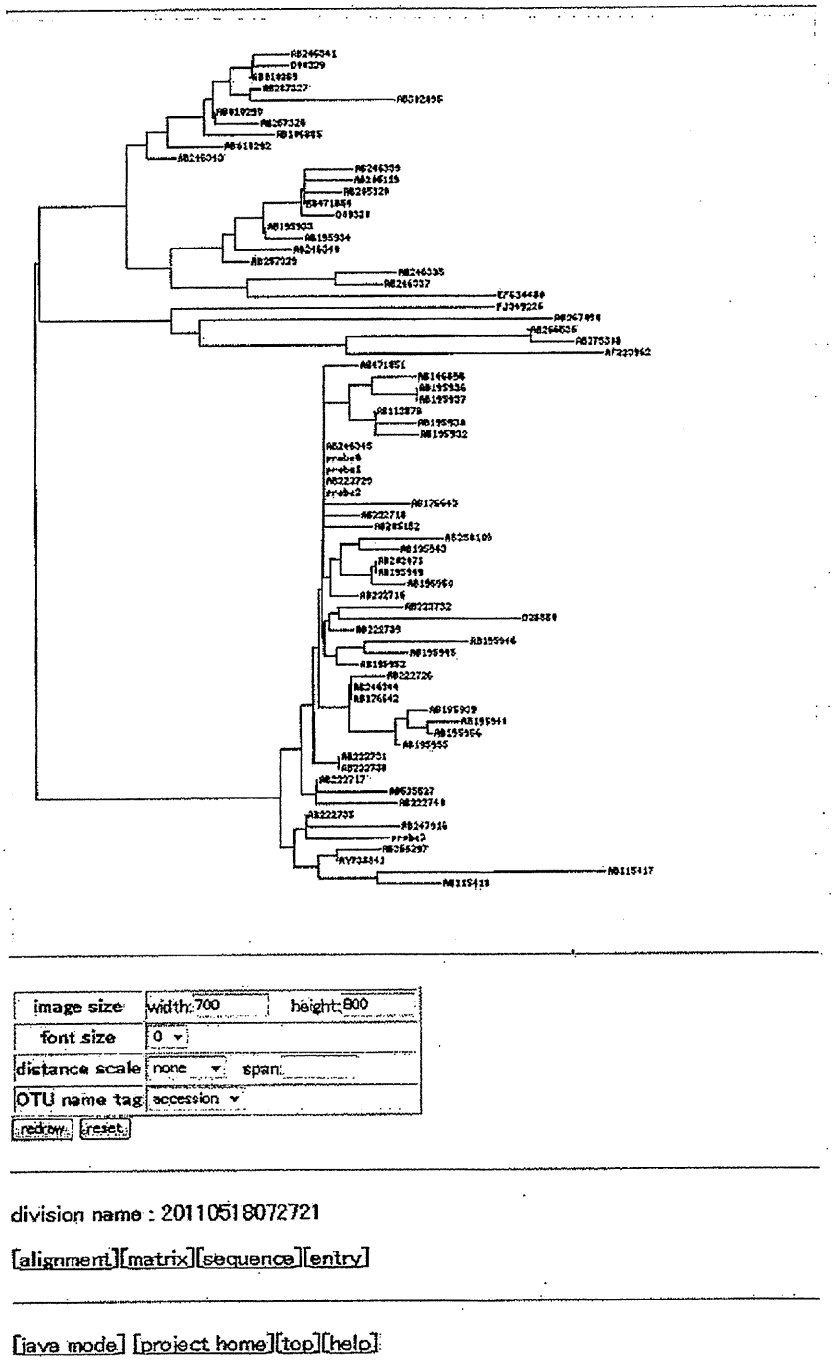

Figure 4 WWW-based user interface and the results of the phylogenetic tree. The phylogenetic tree was calculated based on the matrix data of mismatched nucleotides. A representative result using FM2 data was shown. The character in red indicates the queries. Three members of FM2 had the same sequence in the S region and were classified into the same cluster, whereas sample ID 6 (showed as probe 3 in tree) was classified into another cluster.

The primer set designed in the S region revealed high sensitive amplification because samples with low titer of HBV DNA under the limit of measurement were amplified effectively and the single band was detected in almost all samples by only the 1st PCR. Although we have estimated the substitution rate for HBV to be 4.57×10^{-5} per site per year,[27] the amplified region is a relatively highly conserved area even under antiviral drug pressure[29,30] and the region shows the genotype-dependent sequence. Therefore, a transmission route of sample ID 6 could be divided from that of the other family members. In line with this result, the determination of transmission routes and/or genotyping was achieved sufficiently even if HBV DNA was negative in conventional diagnosis. Therefore, these procedures should be determined with great caution to avoid contamination by trained researchers. The software based on a WWW-browser was customized to fit a Japanese population for quick calculation by reducing entry sequences of foreign origin. Additional datasets are under development because the present system focused on genotype B and C that are originally prevalent in Japan.

This is a versatile tool as the route of suspicious intrafamilial transmission and the genotype were determined in this assay. HBV/A has recently spread out among the young heterosexual population in addition to men who have sex with men.[16,18,19] The determination of transmission routes could contribute to epidemiological research and/or the decision of government policy to prevent the spread of HBV/A. Generally, acute hepatitis B in adulthood becomes chronic in only <1% of cases, which is much less frequent than that in Europe and the United States (approximately 10%). Since HBV/A has been more frequently observed recently in Japan, especially in metropolitan areas, HBV/A infection could provide an increased risk of chronic diseases. Further, HBV/A might be a majority of HBV infection in Japan. Reference sequence of HBV/A registered on this system could be also the appropriate reference for genotyping of HBV/A extracted from Japanese because the HBV/A2 isolates detected in Japan were homologous to those from Europe and the United States in the phylogenetic analysis.[19]

In conclusion, we have developed the easy-to-use system, E-PAS, to determine the transmission route. E-PAS separated one case infected with a clone that was different from the family, which had been expected to be intrafamilial transmission. The system is expected to accelerate the phylogenetic analysis for researchers or physicians who are not familiar with molecular genetics. Although the E-PAS has been primarily developed for Japanese patients, we are planning to extend the application for other patients by collecting foreign samples and reference sequences in addition to improve the calculation method of genetic distance.

ACKNOWLEDGMENTS

THIS WORK WAS supported by a Grant-in-Aid from the Ministry of Health Labor and Welfare of Japan and a Grant-in-Aid for JSPS Fellows of the Ministry of Education, Culture, Sports, Science, and Technology of Japan. The authors thank Professor Takashi Gojobori, National Institute of Genetics and Professor Yoshiyuki Suzuki, Nagoya City University for their professional opinion and technical support. We also thank Ms. Masako Awano, Ms. Miwa Noda, Ms. Ryuko Izumida, Ms. Mikako Kajio, and Ms. Mika Saito for their secretarial support. Laboratory work performed by Ms. Sachiko Sato, Ms. Miki Yoshida, Ms. Chieko Haga, Ms. Mami Ohashi, and Ms. Naomi Nomura is highly appreciated.

REFERENCES

1 Arauz-Ruiz P, Norder H, Robertson BH, Magnius LO. Genotype H: a new Amerindian genotype of hepatitis B virus revealed in Central America. *J Gen Virol* 2002; 83: 2059–73.
2 Chang MH. Impact of hepatitis B vaccination on hepatitis B disease and nucleic acid testing in high-prevalence populations. *J Clin Virol* 2006; 36 (Suppl 1): S45–50.
3 Chen DS. Hepatitis B vaccination: the key towards elimination and eradication of hepatitis B. *J Hepatol* 2009; 50: 805–16.
4 Kao JH, Chen DS. Global control of hepatitis B virus infection. *Lancet Infect Dis* 2002; 2: 395–403.
5 Tada H, Uga N, Fuse Y *et al.* Prevention of perinatal transmission of hepatitis B virus carrier state. *Acta Paediatr Jpn* 1992; 34: 656–9.
6 Stevens CE, Beasley RP, Tsui J, Lee WC. Vertical transmission of hepatitis B antigen in Taiwan. *N Engl J Med* 1975; 292: 771–4.
7 Sung JL, Chen DS. Maternal transmission of hepatitis B surface antigen in patients with hepatocellular carcinoma in Taiwan. *Scand J Gastroenterol* 1980; 15: 321–4.
8 Szmuness W, Prince AM, Hirsch RL, Brotman B. Familial clustering of hepatitis B infection. *N Engl J Med* 1973; 289: 1162–6.
9 Lok AS, Lai CL, Wu PC, Wong VC, Yeoh EK, Lin HJ. Hepatitis B virus infection in Chinese families in Hong Kong. *Am J Epidemiol* 1987; 126: 492–9.

10 Dumpis U, Holmes EC, Mendy M *et al.* Transmission of hepatitis B virus infection in Gambian families revealed by phylogenetic analysis. *J Hepatol* 2001; 35: 99–104.
11 Okamoto H, Tsuda F, Sakugawa H *et al.* Typing hepatitis B virus by homology in nucleotide sequence: comparison of surface antigen subtypes. *J Gen Virol* 1988; 69 (Pt 10): 2575–83.
12 Norder H, Courouce AM, Magnius LO. Complete genomes, phylogenetic relatedness, and structural proteins of six strains of the hepatitis B virus, four of which represent two new genotypes. *Virology* 1994; 198: 489–503.
13 Stuyver L, De Gendt S, Van Geyt C *et al.* A new genotype of hepatitis B virus: complete genome and phylogenetic relatedness. *J Gen Virol* 2000; 81: 67–74.
14 Orito E, Ichida T, Sakugawa H *et al.* Geographic distribution of hepatitis B virus (HBV) genotype in patients with chronic HBV infection in Japan. *Hepatology* 2001; 34: 590–4.
15 Kobayashi M, Ikeda K, Arase Y *et al.* Change of hepatitis B virus genotypes in acute and chronic infections in Japan. *J Med Virol* 2008; 80: 1880–4.
16 Yano K, Tamada Y, Yatsuhashi H *et al.* Dynamic epidemiology of acute viral hepatitis in Japan. *Intervirology* 2010; 53: 70–5.
17 Suzuki Y, Kobayashi M, Ikeda K *et al.* Persistence of acute infection with hepatitis B virus genotype A and treatment in Japan. *J Med Virol* 2005; 76: 33–9.
18 Yotsuyanagi H, Okuse C, Yasuda K *et al.* Distinct geographic distributions of hepatitis B virus genotypes in patients with acute infection in Japan. *J Med Virol* 2005; 77: 39–46.
19 Matsuura K, Tanaka Y, Hige S *et al.* Distribution of hepatitis B virus genotypes among patients with chronic infection in Japan shifting toward an increase of genotype A. *J Clin Microbiol* 2009; 47: 1476–83.
20 Mizokami M, Gojobori T, Lau JY. Molecular evolutionary virology: its application to hepatitis C virus. *Gastroenterology* 1994; 107: 1181–2.
21 Shin IT, Tanaka Y, Tateno Y, Mizokami M. Development and public release of a comprehensive hepatitis virus database. *Hepatol Res* 2008; 38: 234–43.
22 Thompson JD, Higgins DG, Gibson TJ. CLUSTAL W: improving the sensitivity of progressive multiple sequence alignment through sequence weighting, position-specific gap penalties and weight matrix choice. *Nucleic Acids Res* 1994; 22: 4673–80.
23 Gojobori T, Ishii K, Nei M. Estimation of average number of nucleotide substitutions when the rate of substitution varies with nucleotide. *J Mol Evol* 1982; 18: 414–23.
24 Saitou N, Nei M. The neighbor-joining method: a new method for reconstructing phylogenetic trees. *Mol Biol Evol* 1987; 4: 406–25.
25 Locarnini SA, Yuen L. Molecular genesis of drug-resistant and vaccine-escape HBV mutants. *Antivir Ther* 2010; 15: 451–61.
26 Zoulim F, Locarnini S. Hepatitis B virus resistance to nucleos(t)ide analogues. *Gastroenterology* 2009; 137: 1593–608 e1-2.
27 Orito E, Mizokami M, Ina Y *et al.* Host-independent evolution and a genetic classification of the hepadnavirus family based on nucleotide sequences. *Proc Natl Acad Sci USA* 1989; 86: 7059–62.
28 Osiowy C, Giles E, Tanaka Y, Mizokami M, Minuk GY. Molecular evolution of hepatitis B virus over 25 years. *J Virol* 2006; 80: 10307–14.
29 Mizokami M, Orito E, Ohba K, Ikeo K, Lau JY, Gojobori T. Constrained evolution with respect to gene overlap of hepatitis B virus. *J Mol Evol* 1997; 44 (Suppl 1): S83–90.
30 Pallier C, Castera L, Soulier A *et al.* Dynamics of hepatitis B virus resistance to lamivudine. *J Virol* 2006; 80: 643–53.

Nuclear Chk1 prevents premature mitotic entry

Makoto Matsuyama[1,2,*], Hidemasa Goto[1,3,*], Kousuke Kasahara[1,*], Yoshitaka Kawakami[4], Makoto Nakanishi[5], Tohru Kiyono[6], Naoki Goshima[4] and Masaki Inagaki[1,3,‡]

[1]Division of Biochemistry, Aichi Cancer Center Research Institute, Chikusa-ku, Nagoya 464-8681, Japan
[2]The Foundation for Promotion of Cancer Research, Chuo-ku, Tokyo 104-0045, Japan
[3]Department of Cellular Oncology, Graduate School of Medicine, Nagoya University, Showa-ku, Nagoya 466-8550, Japan
[4]Biomedicinal Information Research Center (BIRC), National Institute of Advanced Industrial Science and Technology (AIST), 2-4-7 Aomi, Koto-ku, Tokyo 135-0064, Japan
[5]Biochemistry, Nagoya City University Medical School, Nagoya, Aichi 467-8601, Japan
[6]Division of Virology, National Cancer Center Research Institute, Chuo-ku, Tokyo 104-0045, Japan
*These authors contributed equally to this work
‡Author for correspondence (minagaki@aichi-cc.jp)

Accepted 23 March 2011
Journal of Cell Science 124, 2113-2119

doi:10.1242/jcs.086488

Summary

Chk1 inhibits the premature activation of the cyclin-B1–Cdk1. However, it remains controversial whether Chk1 inhibits Cdk1 in the centrosome or in the nucleus before the G2–M transition. In this study, we examined the specificity of the mouse monoclonal anti-Chk1 antibody DCS-310, with which the centrosome was stained. Conditional Chk1 knockout in mouse embryonic fibroblasts reduced nuclear but not centrosomal staining with DCS-310. In $Chk1^{+/myc}$ human colon adenocarcinoma (DLD-1) cells, Chk1 was detected in the nucleus but not in the centrosome using an anti-Myc antibody. Through the combination of protein array and RNAi technologies, we identified Ccdc-151 as a protein that crossreacted with DCS-310 on the centrosome. Mitotic entry was delayed by expression of the Chk1 mutant that localized in the nucleus, although forced immobilization of Chk1 to the centrosome had little impact on the timing of mitotic entry. These results suggest that nuclear but not centrosomal Chk1 contributes to correct timing of mitotic entry.

Key words: Cdk1, Centrosome, Chk1, Nucleus, G2–M transition

Introduction

The cell division cycle is a tightly regulated set of events to distribute complete and accurate replicas of the genome to daughter cells. Checkpoints monitor DNA replication and repair, and thereby couple the completion of these events to the onset of mitosis. In the center of these pathways, there exists a protein kinase cascade from ataxia-telangiectasia and Rad3-related (ATR) to Chk1, the activation of which requires ssDNA and several nuclear proteins, such as replication protein A (RPA), ATR interacting protein (ATRIP), Rad9-Rad1-Hus1 (9-1-1) checkpoint complex, topoisomerase (DNA) II binding protein 1 (TOPBP1), and claspin (Zhou and Elledge, 2000; Chini and Chen, 2004; Kastan and Bartek, 2004; Cimprich and Cortez, 2008; Reinhardt and Yaffe, 2009). ATR phosphorylates Chk1 at Ser317 and Ser345, which then induces autophosphorylation of Chk1 at Ser296. These phosphorylation events are required for the transmission of checkpoint signals to downstream effectors (Zhao and Piwnica-Worms, 2001; Walker et al., 2009; Kasahara et al., 2010). With regard to the cell cycle arrest, Chk1 phosphorylates and inactivates members of the Cdc25 family of dual specificity phosphatases (Neely and Piwnica-Worms, 2003; Boutros et al., 2007). Since these enzymes control cyclin-B1–Cdk1 activation through the dephosphorylation of Thr14 and Tyr15 in the ATP-binding loop of Cdk1 (Nigg, 2001; Doree and Hunt, 2002; Nurse, 2002), activation of Chk1 eventually blocks premature mitotic entry (Lindqvist et al., 2009).

Recent studies have also demonstrated that Chk1 prevents Cdk1 from unscheduled activation even in an unperturbed cell cycle (Kramer et al., 2004; Enomoto et al., 2009). Two models were proposed to explain how Chk1 shields Cdk1 from premature activation. In one model, centrosome-associated Chk1 prevents premature activation of Cdk1 (Kramer et al., 2004; Tibelius et al., 2009). By using the anti-Chk1 monoclonal antibody DCS-310, Kramer and colleagues reported that Chk1 localized to centrosomes in interphase cells but not in prophase cells (Kramer et al., 2004). The 8-day stable induction of GFP-Chk1–PACT (pericentrin-AKAP450 centrosomal targeting domain) inhibited the G2–M transition. Based on these data, they proposed that Chk1 dissociates from the centrosome at the G2–M transition and then cyclin-B1–Cdk1 is activated on the centrosome (Kramer et al., 2004; Tibelius et al., 2009). This centrosomal model is well fit for the observation that active cyclin-B1–Cdk1 was first detected on the centrosome (Jackman et al., 2003). In the other model, nuclear Chk1 prevents premature activation of Cdk1 (Enomoto et al., 2009). By using three independent anti-Chk1 monoclonal antibodies including DCS-310, we have previously demonstrated that Chk1 translocates from the nucleus to the cytoplasm at the G2–M transition (Enomoto et al., 2009). This translocation is regulated by Cdk1-induced Chk1 phosphorylation at Ser286 and Ser301 (Shiromizu et al., 2006), and disturbance of this process results in a delay in mitotic entry (Enomoto et al., 2009). Thus, we have proposed a model in which Cdk1-induced Chk1 phosphorylation leads to the elimination of active Chk1 kinase from the nucleus, which triggers a positive feedback loop of Cdk1 activation in the nucleus. This nuclear model is fits well the observation that Chk1 activation occurs predominantly in the nucleus (Sanchez et al., 1997; Jiang et al., 2003).

The spatiotemporal regulation of several protein kinase activities is considered to have crucial roles in the coordination of

centrosomal, cytoplasmic, and nuclear events during cell cycle progression and checkpoints (Nigg, 2001; Reinhardt and Yaffe, 2009). Since the centrosome is considered to be a hub in which the cyclin-B1–Cdk1 complex is first activated (Jackman et al., 2003), the centrosomal Chk1 model is attractive. However, this centrosomal model is based largely on the use of one anti-Chk1 antibody, DCS-310 (Kramer et al., 2004; Tibelius et al., 2009). In this present study, we show that the centrosomal reactivity of this antibody reflects the crossreactivity with another protein, Ccdc151, and that Chk1 does not localize to the centrosome. In addition, forced localization of Chk1 to the centrosome has little effect on the entry into mitosis, whereas forced nuclear transport caused a delay in mitotic entry.

Results and Discussion

Chk1 is localized predominantly in the nucleus but not on the centrosome

An anti-Chk1 monoclonal antibody DCS-310 is reported to react with the centrosome in cells fixed with methanol:acetone (1:1) (Kramer et al., 2004; Tibelius et al., 2009). We confirmed that DCS-310 reacts with the centrosome in cells fixed with methanol:acetone (1:1) (Fig. 1B and Fig. 3D) or 1% formaldehyde (Fig. 2E) but not with 3.7% formaldehyde (not depicted). However, especially in methanol–acetone-fixed cells (Fig. 1B and Fig. 3D), nuclear and cytoplasmic DCS-310 signals are much weaker than in cells fixed with 3.7% formaldehyde (Enomoto et al., 2009). In the experiments described here, we used cells fixed in methanol:acetone (1:1) or 1% formaldehyde to evaluate centrosomal DCS-310-staining.

We used Chk1$^{flox/-}$ mouse embryonic fibroblasts (MEFs) in which one *lox*-flanked (flox) *Chk1* allele can be converted into a null allele by Cre–*lox* site-specific homologous recombination (Niida et al., 2005) to examine the effect of conditional Chk1 knockout on the DCS-310-immunoreactivity. For this purpose, we infected Chk1$^{flox/-}$ MEFs with an adenovirus carrying either β-galactosidase (Ad-LacZ; the infection control) or Cre recombinase (Ad-Cre) as described previously (Shimada et al., 2008) and then analyzed them 3 days after the infection. As shown in Fig. 1A, we detected a 54-kDa band that corresponds to mouse Chk1 in the MEFs infected with Ad-LacZ but not with Ad-Cre, demonstrating the success of conditional Chk1 knockout. As shown in Fig. 1B, nuclear and cytoplasmic DCS-310 signals were decreased in Chk1$^{\Delta/-}$ MEFs (infected with Ad-Cre), compared with Chk1$^{flox/-}$ MEFs (infected with Ad-LacZ). However, we observed only marginal differences in the centrosomal staining between these two cells (Fig. 1B); a similar tendency was observed using MEFs fixed with 1% formaldehyde (not shown). These results suggest that, at least on the centrosome, DCS-310 crossreacts with protein(s) other than Chk1.

We next replaced one *CHK1* allele with Myc-tagged Chk1 in stable human colon adenocarcinoma (DLD-1) cells (Fig. 2). As shown in Fig. 2A, we performed homology-directed gene replacement with recombinant adeno-associated virus (rAAV) vector (Kohli et al., 2004; Rago et al., 2007). One *CHK1* allele was targeted by rAAV infection, drug selection and screening by PCR. We confirmed the isolation of heterozygotes, Chk1$^{+/myc}$ cell clones by Southern blot hybridization (Fig. 2B) and by western blotting (Fig. 2C). We treated Chk1$^{+/myc}$ cells with hydroxyurea (HU) in order to activate the DNA replication checkpoint (Fig. 2D). Like wild-type Chk1, Myc-Chk1 (lower and upper bands, respectively) was phosphorylated at Ser345 in HU-treated cells (Fig. 2D), confirming that Myc-Chk1 expressed in DLD-1 cells was functional. In DLD-1$^{+/myc}$ cells fixed with 1% formaldehyde, the nucleus was strongly stained not only by DCS-310 but also anti-

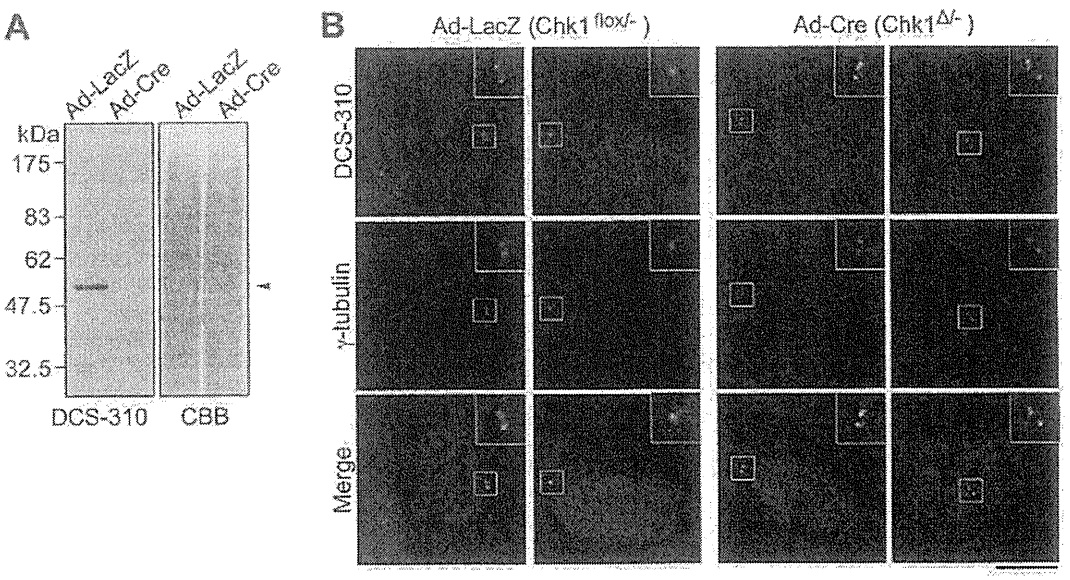

Fig. 1. The centrosome stained positive for Chk1 with the monoclonal antibody DCS-310, even after conditional Chk1 knockout. (**A**,**B**) Chk1$^{flox/-}$ MEFs (Niida et al., 2005) were infected with adenovirus carrying β-galactosidase (Ad-LacZ; infection control) or Cre recombinase (Ad-Cre), as described previously (Shimada et al., 2008). At 3 days after infection, cells were subjected to western blotting (A) or immunocytochemistry (B) with DCS-310. After blotting, transferred membrane was stained with Coomassie Brilliant Blue (CBB; A). Cells were co-stained with anti-γ-tubulin (to detect centrosomes) and DAPI (to detect nuclei; B). Boxed areas (top right) in B show the indicated centrosomes at high magnification. Scale bar: 5 μm